OPTIMAL DESIGN OF CENTRIFUGAL COMPRESSORS IN SMALL-SIZE HIGH-TEMPERATURE BRAYTON HEAT PUMPS

Guido Francesco Frate[1]*, Matteo Benvenuti[1], Francesco Chini[1], Lorenzo Ferrari[1]

[1]University of Pisa, Department of Energy, Systems, Territory and Construction Engineering, Pisa, Italy

*Corresponding Author: guido.frate@unipi.it

ABSTRACT

High-temperature heat pumps (HTHP) are becoming a commercial solution to electrify and decarbonise industrial heat production by converting the power produced by renewable energy sources into thermal energy at suited temperature levels. Commercial technologies, mostly Rankine-based, are limited to up to 200 °C, but higher temperatures may be achieved using Brayton HTHP. These devices usually operate according to an inverse and internally recuperated Brayton cycle, where the compressor operates at temperatures higher than the standard values, which requires adapting current designs to the new operating condition ranges. The analysis focuses on small-scale Brayton HTHPs that operate in a range of pressures, mass flow rates and power inputs suited to centrifugal compressors. For this compressor technology, a fast and flexible software tool to preliminarily optimise the geometrical design according to the machine inlet and operating conditions is developed and validated in the paper. After presenting the model, its assumptions and validation, the paper maps the main geometrical features and overall performance of the optimised compressors in a range of operating conditions representative of HTHP applications. This way, the main drivers for the centrifugal compressor performance are investigated, and design guidelines adapted to HTHP applications are provided.

1 INTRODUCTION

Fossil fuels are the industry's primary source of heat generation, and the related decarbonisation process may pose significant technical, economic, and societal issues (Manuel et al., 2022). Nonetheless, such decarbonisation will occur, and one proposed strategy to achieve it relies on heat production electrification, which can be done in various ways, from introducing electric heaters/boilers to integrating High-Temperature Heat Pumps (HTHP) and mechanical vapour recompression into the industrial processes (Bless et al., 2017).

Focusing on HTHP, they can provide heat at different temperature levels in chemical, food, metal, and paper industries (Arpagaus et al., 2018), but their spreading is constrained by economic and technical barriers (Schlosser et al., 2020). One such barrier is the inability to operate efficiently above 200 °C and with temperature lifts above 100 K (Bergamini et al., 2019), even though several industrial sectors show a potential demand for HTHP operating up to these or even higher ranges (Marina et al., 2021).

Heat pump systems based on reverse Brayton cycles may easily overcome the technological limitations affecting HTHPs, primarily based on vapour compression architectures (Arpagaus et al., 2018). Even though Brayton HTHP show lower COP compared to vapour compression systems for the same temperature lifts, they feature an unmatched capability to operate at very high temperatures and lifts. For example, in (Gollasch et al., 2024), the authors investigated a Brayton HTHP, finding that a COP comprised between 1.65 and 1.75 is expected while operating at 320 °C, with a lift of 240 K.

Other positive features of Brayton HTHP include the possibility of producing sensible heat (Gai et al., 2020), the use of clean and safe operating fluids (such as Air, Argon, Nitrogen and CO_2) and part-load flexibility due to the use of inventory control (Gollasch et al., 2024).

Even though many authors agree that Brayton HTHP is the best alternative to produce heat at temperatures above 200 °C, from technical and thermodynamic points of view, these systems may struggle to achieve economic feasibility (Zühlsdorf et al., 2019). It is, therefore, mandatory to focus on

https://doi.org/10.52202/077185-0031

simple, compact, and cheap layouts to promote the economic viability of HTHP. This means, for example, operating with open cycles, eliminating the need for a heat exchanger between the cycle fluid and the environment. For heat exchangers, this implies limiting the dimensions of the selected components to realistic values, i.e. thermal effectiveness up to 0.85 or 0.9, depending on the fluids involved, as suggested in (Gollasch et al., 2024), even though this may introduce non-negligible penalties on the COP (White, 2009). For the machines, this may imply resorting to straightforward designs, e.g. using single-stage machines. This may be possible only for small systems, on a few hundred thermal kWth scale, for which the involved mass flow rates do not require axial compressors. Of course, similar design limitations (heat exchangers of limited effectiveness and single-stage compressors) may reduce the COP and, in general, the applicability of the Brayton HTHP.

This paper investigates a small-scale (100 kWth) Brayton HTHP system to identify the maximum achievable COP when practical heat exchanger dimensions and simple compressor designs (single stage) are imposed. An analytical model of the HTHP cycle was developed to identify the compressor's design specifications (inlet condition, mass flow rate and pressure ratio). Some cycle configurations of practical interest were selected, and a detailed compressor design was produced for each, using a detailed 1-D model validated against experimental data taken from the literature.
The model was used to estimate the compressor capabilities in terms of pressure ratio and isentropic efficiency, two crucial parameters for the Brayton HTHP performance maximisation. Since these two quantities are often conflicting (the maximisation of one leads to the minimisation of the other), the compressor design was formulated as a multiobjective optimisation problem. Finally, the results provided helpful insights into the performance that small-scale Brayton HTHP can realistically achieve. Furthermore, the developed compressor model may represent a crucial stepping stone for further developing advanced analysis and design methodologies for Brayton HTHP cycles.

2 METHODOLOGY

2.1 Thermodynamic modelling of the heat pump cycle

In the analysis, an open-cycle and internally regenerated Brayton HTHP is studied (Figure 1). In the hypotheses of constant specific heat (ideal and perfect gas), negligible pressure drops in the heat exchangers and negligible heat leakages from each component, the COP analytical expression can be derived with simple but tedious calculations not reported here:

$$COP = \frac{\varepsilon_{ihx}[(\eta_{is}^t K_2+1)(\eta_{is}^c+2K_1)T_{max}-(\eta_{is}^c+K_1)T_{min}]+(\eta_{is}^c+K_1)[T_{min}-(\eta_{is}^t K_2+1)T_{max}]}{2\varepsilon_{ihx}[T_{max}K_1(\eta_{is}^t K_2+1)+T_{min}\eta_{is}^t K_2(\eta_{is}^c+K_1)]-T_{max}K_1(\eta_{is}^t K_2+1)-T_{min}\eta_{is}^t K_2(\eta_{is}^c+K_1)} \quad (1)$$

With $K_1 = PR^{(k-1)/k} - 1$ and $K_2 = PR^{(1-k)/k} - 1$. The COP may be calculated according to the compressor (η_{is}^c) and turbine (η_{is}^t) isentropic efficiencies, cycle pressure ratio (PR), cycle minimum and maximum temperatures (T_{max} and T_{min}, equal to T_b and T_e in Figure 1) and internal heat exchanger effectiveness ε_{ihx}. Not all arbitrary combinations of these values yield physically meaningful cycles. In particular, for any combination of η_{is}^c, η_{is}^t, PR, T_{max} and T_{min} a unique value of ε_{ihx} exists such that $T_f = T_{env}$ (as it should be in an open cycle), which can be numerically determined from cycle equations. In the analysis, different values of T_{max}, T_{min} and PR are explored to estimate the COP in different configurations. Differently, for machine efficiencies, constant values are assumed during the cycle analysis: $\eta_{is}^c = 0.8$ and $\eta_{is}^t = 0.9$. Finally, a thermal production $\dot{Q}_{sink} = 100$ kW is assumed.

Solving the cycle equations allows for determining the HTHP operating conditions, including the COP, the cycle mass flow rate and the machine inlet conditions. These quantities may be used to define the machines' design specifications and asses, using a dedicated simulation procedure, the impact of such specifications on the machine design. In this paper, a detailed design of the compressor is presented, while it is assumed that the turbine is capable of achieving the prescribed efficiency ($\eta_{is}^t = 0.9$).

https://doi.org/10.52202/077185-0031

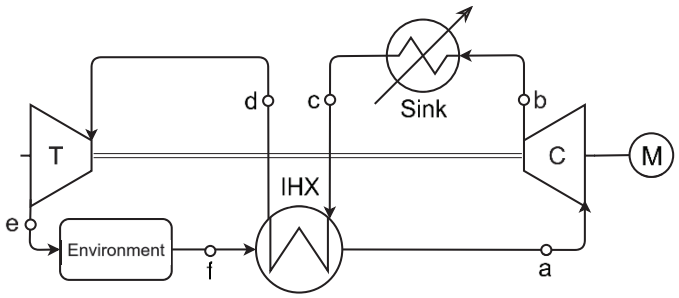

Figure 1: Open-cycle (i.e., air is the operating fluid) Brayton HTHP layout with internal regeneration.

2.2 Compressor Model

This section will describe the compressor model outlined in Figure 2 (b). Regarding the compressor, a reference is made to the machine geometry reported in Figure 2 (a), where it is possible to observe all the characteristic sections of the compressor. They are identified as follows: (1) the impeller inlet section, (1*) the impeller throat section, (2) the impeller outlet section, (3) the vaneless diffuser outlet section, (4) the volute outlet section and finally, (5) the cone outlet section (not represented in the figure).

The model characteristics are in line with 1-D state-of-the-art models, e.g., those presented in (Meroni et al., 2018) and (Unterluggauer et al., 2023) for vapour compression systems. The model was implemented in Matlab and can be downloaded at the link provided in the Supplementary Materials section.

Firstly, the model input parameters are reviewed. These parameters are related to the impeller's geometry and the fluid's inlet thermodynamic conditions and include the impeller radii at the inlet shroud and hub r_{1s} and r_{1h} and at the outlet r_2, the blade height at the outlet b_2, the vaneless diffuser radial extend r_3, the blade geometric angle at the impeller inlet – at the root mean square (rms) radius – and outlet $\beta_{1rms,b}$ and $\beta_{2,b}$. All the other relevant dimensions can be calculated or reasonably assumed from these. The inlet flow is purely axial (no IGV is considered, $\alpha_1 = 0$). The impeller axial length is calculated as $L_z = 0.4(2r_2 - r_{1s} + r_{1h})$ (Meroni et al., 2018). The ratio between the radial position of the centre of the volute outlet section and the diffuser radial dimension r_4/r_3 is fixed and equal to 1.4. Similarly, the cone length is assumed as $L_c = 1.2r_3$, and its divergence angle is set to 5° (Aungier, 2000). The number of blades is calculated as $N_b = 12.03 + 2.544\, PR_{tt}$ (Xu and Amano, 2012). Regarding the thermodynamic conditions, the total pressure p_{01} and temperature T_{01} are considered. In addition, it is necessary to provide the rotational speed of the machine Ω in RPM, and the mass flow rate $\dot{m}$ in kg/s. The thermophysical properties of the fluid (e.g., c_p, c_v, $k = c_p/c_v$, viscosity) are calculated with CoolProp (Bell et al., 2014) at the impeller inlet and maintained constant along the entire compressor (ideal and perfect gas hypotheses). With this in mind, it is possible to analyse the various sections.

Regarding the inlet section (1), the root-mean-square (rms) radius is defined as the radius dividing the passage into two regions with the same flow rate $r_{1rms} = [0.5(r_{1h}^2 + r_{1s}^2)]^{-0.5}$ (Casey and Robinson, 2021). The thermodynamic conditions were calculated by solving the following set of equations iteratively since the density's exact value is unknown (as the inlet velocity is unknown):

$$c_1 = \frac{\dot{m}}{\rho_1 A_1} \tag{2}$$

$$T_1 = T_{01} - \frac{c_1^2}{2c_p} \tag{3}$$

$$Ma_1 = c_1/\sqrt{kRT_1} \tag{4}$$

$$p_1 = p_{01}/\left(1 + \frac{k-1}{2} Ma_1^2\right)^{\frac{k}{k-1}} \tag{5}$$

$$\rho_1 = p_1/(RT_1) \tag{6}$$

https://doi.org/10.52202/077185-0031

By knowing c_1, the rotational speed and the radius, section 1 velocity triangle can be solved. In correspondence with the inlet section, attention must be paid to the calculation of the velocity vectors $\vec{w}$ and $\vec{u}$, which will all differ due to the radius variation between the hub, rms and shroud. The flow and blade constructive angles are calculated by considering the hub and shroud's velocity triangles with c_1 being constant along the radius. From p_1, T_1 and c_1 the enthalpy and entropy can be calculated.

After the inlet section, the throat section (1*) is examined. The throat flow area was approximated as the sum of two trapezoids (Casey and Robinson, 2021). From the inlet to the throat, constant stagnation enthalpy was assumed ($h_{01} = h_{01*}$), it is assumed that this transition is isentropic ($p_{01} = p_{01*}$), that the $\vec{u}$ remains constant ($\vec{u}_1 = \vec{u}_{1*}$), and that the relative velocity $\vec{w}_{1*}$ is perpendicular to the passage section and follows the direction imposed by the blade (blade angles are used in the calculations) (Meroni et al., 2018). With these hypotheses, a new iterative calculation over the density is performed:

$$w_{1*} = \frac{\dot{m}}{\rho_{1*} A_{1*}} \tag{7}$$

With w_{1*}, section 1* velocity triangle can be solved, and c_{1*} can be calculated. With this:

$$h_{1*} = h_{01} - c_{1*}^2/2 \tag{8}$$
$$T_{1*} = h_{1*}/c_p \tag{9}$$
$$Ma_{1*} = c_{1*}/\sqrt{kRT_{1*}} \tag{10}$$
$$p_{1*} = p_{01}/\left(1 + \frac{k-1}{2} Ma_{1*}^2\right)^{\frac{k}{k-1}} \tag{11}$$
$$\rho_{1*} = p_{1*}/(RT_{1*}) \tag{12}$$

From p_{1*}, T_{1*} and c_{1*} the entropy and all the thermophysical properties in section 1* can be calculated.

After the throat section, the analysis proceeds to section 2 (impeller exit). The impeller exit's conditions are evaluated by solving the following equations. For velocities, the following expressions hold:

$$c_{2m} = \frac{\dot{m}}{\rho_2 A_2} \tag{13}$$
$$c_{2u} = \sigma u_2 - c_{2m} \tan\left(\left|\beta_{2,b}\right|\right) \tag{14}$$

The section 2 velocity triangle can be solved with these velocities, and all the other velocity components and flow angles can be calculated. The slip factor σ is evaluated as in (Wiesner, 1967) with the correction of (Aungier, 2000) as discussed in (Meroni et al., 2018). With the velocities, the thermodynamic conditions are then calculated:

$$h_{02} = h_{01} + u_2 c_{2u} - u_{1rms} c_{1u} \tag{15}$$
$$h_2 = h_{02} - c_2^2/2 \tag{16}$$
$$T_2 = h_2/c_p \tag{17}$$

The impeller outlet pressure is determined from the isentropic outlet conditions by removing the losses internal to the impeller (Δh_{int}):

$$h_{02,is} = h_{02} - \Delta h_{int} \tag{18}$$

The correlations indicated by (Meroni et al., 2018) are used for the impeller losses. Losses are categorised into internal losses and parasitic – external – losses ((Oh et al., 1997) (Zhang et al., 2019)), with the second not resulting in a pressure increase despite a total enthalpy loss. Internal losses are due to *incidence, skin friction, blade loading*, and *clearance*. In contrast, parasitic losses are *mixing, disk friction,* and *recirculation* losses. From $h_{02,is}$, it is possible to derive all the thermodynamic conditions of the isentropic outlet including static pressure:

$$T_{02,is} = h_{02,is}/c_p \tag{19}$$

https://doi.org/10.52202/077185-0031

$$T_{2,is} = T_{02,is} - \frac{c_2^2}{2c_p} \quad (20)$$

$$p_{02,is} = p_{01}\left(T_{02,is}/T_{01}\right)^{k/(k-1)} \quad (21)$$

$$p_2 = p_{02,is}\left(T_{02,is}/T_{2,is}\right)^{k/(1-k)} \quad (22)$$

$$\rho_2 = p_2/(RT_2) \quad (23)$$

From p_2, T_2 and c_2 the entropy and all the remaining thermophysical properties can be calculated.

Next, the vaneless diffuser is analysed (section 3), where total enthalpies and temperatures are conserved ($h_{02} = h_{03}$ and $T_{02} = T_{03}$). In the vaneless diffuser, the free vortex law ($c_u \cdot r = cost$) is corrected to include friction-related losses (Δh_{vld}) (Khoshkalam et al., 2019), which allows calculating the tangential component of c_3, i.e. c_{3u}. The set of equations describing the vaneless diffuser:

$$c_{3m} = \dot{m}/(\rho_3 A_3) \quad (24)$$

$$c_{3u} = c_{2u}/\left[\frac{r_3}{r_2} + \frac{2\pi C_f \rho_2 c_{2u} * \left(r_3^2 - r_2 r_3\right)}{\dot{m}}\right] \quad (25)$$

$$c_3 = \sqrt{c_{3m}^2 + c_{3u}^2} \quad (26)$$

$$h_3 = h_{03} - c_3^2/2 \quad (27)$$

$$T_3 = h_3/c_p \quad (28)$$

$$h_{03,is} = h_{03} - \Delta h_{vld} \quad (29)$$

$$T_{03,is} = h_{03,is}/c_p \quad (30)$$

$$p_{03,is} = p_{02}\left(T_{02}/T_{03,is}\right)^{k/(1-k)} \quad (31)$$

To pass from $p_{03,is}$ to p_3 the velocity that the fluid would have in the absence of losses (c_{3is}) must be used and not c_3, which can be calculated by solving the following equations:

$$c_{3m,is} = \dot{m}/\left(\rho_{3,is} A_3\right) \quad (32)$$

$$c_{3u,is} = c_{2u} r_2/r_3 \quad (33)$$

$$c_{3,is} = \sqrt{c_{3m,is}^2 + c_{3u,is}^2} \quad (34)$$

$$T_{3,is} = T_{03} - \frac{c_{3,is}^2}{2c_p} \quad (35)$$

$$p_3 = p_{03,is}\left(T_{03,is}/T_{3,is}\right)^{k/(1-k)} \quad (36)$$

$$\rho_{3,is} = p_3/\left(RT_{3,is}\right) \quad (37)$$

With p_3, which is the same for isentropic and actual outlet conditions (by definition), ρ_3 is calculated:

$$\rho_3 = p_3/(RT_3) \quad (40)$$

For the volute (section 4), the following set of equations is solved by remembering that total enthalpies and temperatures are conserved ($h_{04} = h_{03}$ and $T_{04} = T_{03}$) and by modelling the total pressure loss with the factor K_{vlt} as in (Aungier, 2000).

$$c_4 = \frac{\dot{m}}{\rho_4 A_4} \quad (41)$$

$$T_4 = T_{04} - \frac{c_4^2}{2c_p} \quad (42)$$

$$p_{04} = p_{03} - (p_{03} - p_3) K_{vlt}$$

$$Ma_4 = c_4/\sqrt{kRT_4} \quad (43)$$

$$p_4 = p_{04}/\left(1 + \frac{k-1}{2} Ma_4^2\right)^{\frac{k}{k-1}} \quad (44)$$

$$\rho_4 = p_4/(RT_4) \quad (45)$$

https://doi.org/10.52202/077185-0031

The total pressure losses are converted to total enthalpy losses (Δh_{vlt}) utilising the average density between sections 3 and 4. The volute losses encompass the meridian velocity loss, tangential velocity loss and skin friction.

For the exit cone, the solving is analogous to what was presented for the volute. The total pressure loss factor is again evaluated according to (Aungier, 2000) and converted to total enthalpy losses (Δh_{cone}) with the average density between sections 4 and 5.

The compressor performance parameters relevant to the HTHP cycle are the total-to-static isentropic efficiency:

$$\eta_{ts} = (h_{02} - h_{01} - \Delta h_{int} - \Delta h_{vld} - \Delta h_{vlt} - \Delta h_{cone} - c_5^2/2\,)/(h_{02} - h_{01} + \Delta h_{ext}) \tag{46}$$

And the total-to-static pressure ratio:

$$PR_{ts} = p_5/p_{01} \tag{47}$$

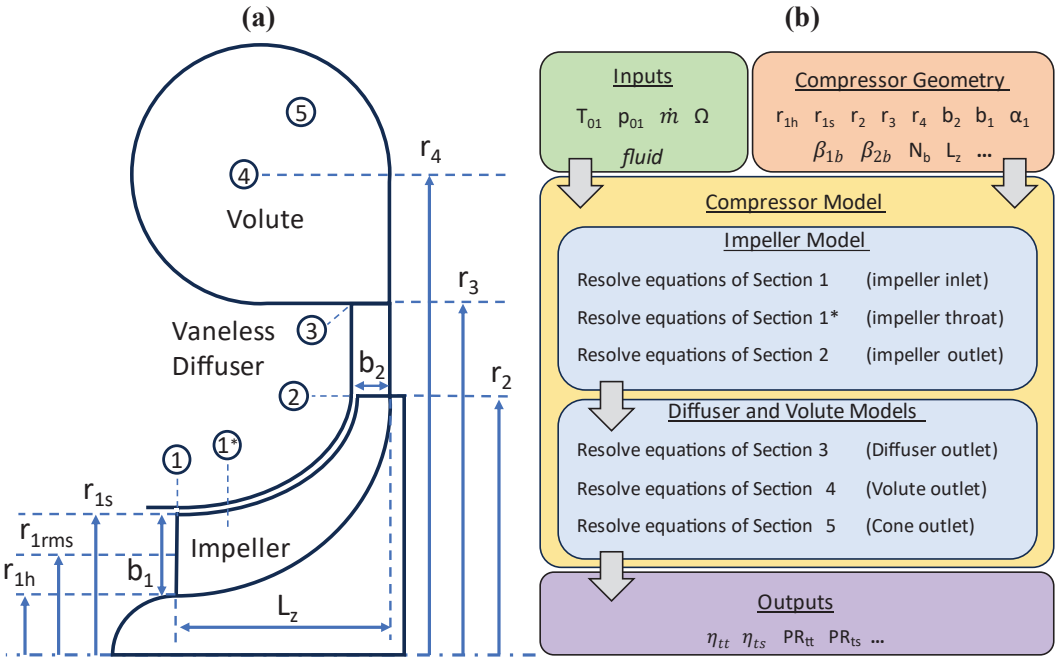

Figure 2: Compressor modelling details. (a): Compressor geometry. (b): Model structure.

2.1 Compressor Model Validation

The compressor model was validated against experimental data taken from the literature. The data are related to the well-known Eckardt compressors, often used in the literature for validating 1D compressor models (Oh et al., 1997; Meroni et al., 2018).

The comparison between the model predictions and the experimental data is reported in Figure 3. The model yielded satisfactory performance, as most total-to-total pressure ratios and isentropic efficiency values have been predicted with a relative error lower than ±5% for all three compressors. The model accuracy in predicting the isentropic efficiency is lower than that of pressure ratios. However, the points predicted with errors above ±10% are relatively few compared to the total.

Finally, the model relative errors were calculated for all the points in Figure 3, estimating the 5th and 95th percentiles of their distribution, which will be used as error bars in the discussion of the results.

https://doi.org/10.52202/077185-0031

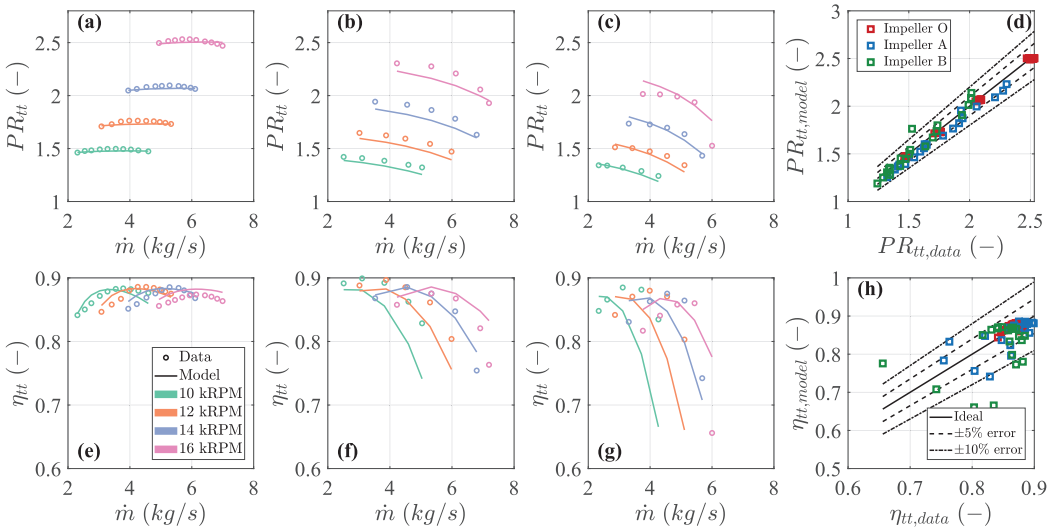

Figure 3: Compressor model validation versus experimental data of Eckart compressors (Impeller O in panels (a) and (e), Impeller A in panels (b) and (f), and Impeller B in panels (c) and (g)). Data from (Meroni et al., 2018). (a) to (c): PR_{tt} from model and experiments for various rotating speeds. (e) to (g): η_{tt} from the model and experiments for various rotating speeds. (d) and (h): Parity plots for PR_{tt} and η_{tt} for the three compressors.

2.2 Compressor geometry optimisation

In the paper, the compressor's design specifications have been optimised to find the compressor with the best performance given the operating fluid and inlet conditions. The vector $\vec{x}$ of the optimisation variables is defined as follows:

$$\vec{x} = \{\Omega,\ r_2,\ r_{1s}/r_2\,,\ r_{1h}/r_2\,,\ b_2/r_2\,,\ r_3/r_2\,,\ \beta_{1rms,b},\ \beta_{2,b}\} \tag{48}$$

The impeller radius r_2 is limited according to Ω to avoid impeller exit peripheral speeds over 400 m/s to limit the blade mechanical stress (Meroni et al., 2018), while the other optimisation variables vary within lower and upper boundaries to find manufacturable, physically meaningful, and technically feasible solutions. Since the objective of the compressor design is to achieve not only the best efficiency but also the desired pressured ratio, and the two objectives are conflicting, the optimization problem can be solved as a multiobjective one, where the two objectives are the total-to-static isentropic efficiency and pressure ratio. The optimisation problem can be formally stated as:

$$\min_{\vec{x}}[PR_{ts}(\vec{x}),\ \eta_{ts}(\vec{x})] \tag{49}$$

which was solved in a scalarised form utilising the technique based on reference points (targets) proposed by (Wierzbicki, 1980).

3 RESULTS

3.1 Results related to the analytical cycle analysis

In Figure 4, the results related to the cycle analysis for T_{max} = 300 °C are presented. By analysing the maps in Figure 4(b), it emerges that the COP tends to grow by lowering T_{min} and PR, which is positive as low-pressure ratios usually yield more efficient compressor designs and lower heat exchanger costs due to limited mechanical stress on the high-pressure side. However, from the T-s diagram in Figure 4(b), it can be understood that for fixed values of T_{max} and PR, lower T_{min} values can only be achieved by increasing the internal heat exchanger's effectiveness ε_{ihx}. Therefore, larger COP can only be

https://doi.org/10.52202/077185-0031

achieved for high ε_{ihx}, which may entail extensive heat exchangers, considering that the hot and cold fluids are low-pressure gasses (air) that tend to have low heat transfer coefficients.

Several studies agree on the fact that $\varepsilon_{ihx} = 0.8$ represents a practical and somewhat conservative recuperator design (White, 2009; Walden et al., 2023; Gollasch et al., 2024) and will be assumed as a reference in the paper. The configurations with $\varepsilon_{ihx} = 0.8$ are clearly identified by the red line, which shows how, if practical ε_{ihx} values are assumed, the feasible design combinations (those with $\varepsilon_{ihx} \leq 0.8$) are greatly restricted and the resulting COP values are limited to values lesser than 1.45 (which still represent a remarkable value for the envisioned application).

Besides the COP, Figure 4(b) also shows that the trend of $\dot{Q}_{sink}/\dot{m}$ is different from that of the COP. Even though this parameter does not directly impact the cycle performance, it is crucial for the compressor design, as it links the two essential design specifications: the pressure ratio and the mass flow rate.

As it resulted, $\dot{Q}_{sink}/\dot{m}$ increases by simultaneously increasing PR and lowering T_{min}. This is approximately the direction followed by the lines with a constant ε_{ihx}, meaning that the configurations with $\varepsilon_{ihx} = 0.8$ and high COP, achieved by simultaneously increasing PR and lowering T_{min} *along* the $\varepsilon_{ihx} = 0.8$ line, have a comparatively high coefficient of performance and a low mass flow rate. Therefore, when ε_{ihx} is fixed, COP and mass flow rate have opposite trends: when the first increases, the second decreases and vice versa.

Finally, to test the practical feasibility of the proposed HTHP configurations with single-stage compressor designs, five configurations along the line with $\varepsilon_{ihx} = 0.8$ have been selected. The related data are reported in Table 1.

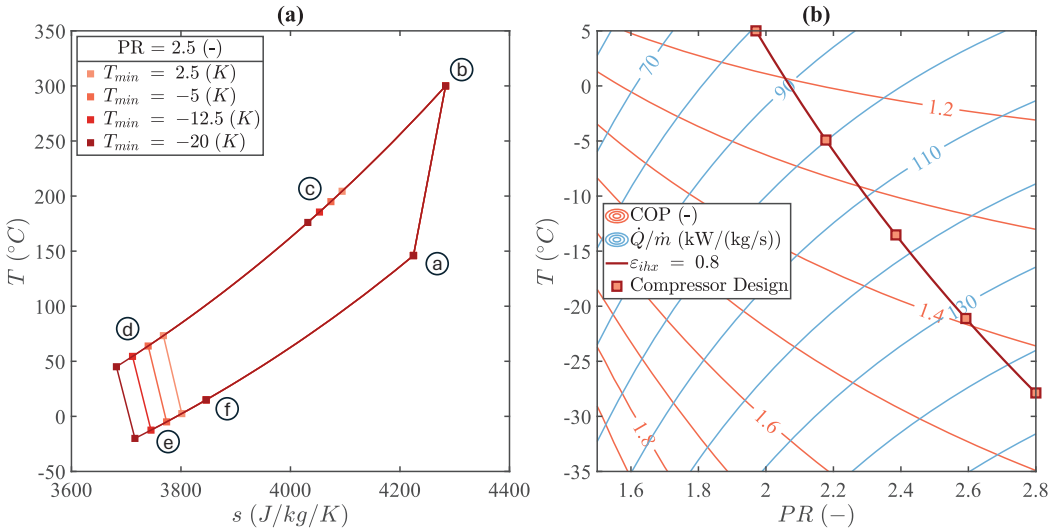

Figure 4: Analysis of the thermodynamic cycles operating with air and T_{max} = 300 °C. (a): Some examples of thermodynamic cycles in the T-s diagram for PR = 2.5 and various cycle T_{min}. (b): Trend of heat pump COP and specific heat production ($\dot{Q}_{sink}/\dot{m}$) for various combinations of PR and T_{min} and five selected cycle configurations with ε_{ihx} = 0.8.

Table 1: Design specifications for the compressor design. p_0 = 1 bar and T_{out} = 300 °C

COP (-)	PR (-)	$\dot{Q}_{sink}/\dot{m}$ (kW/(kg/s))	T_{in} (°C)
1.15	1.97	80.6	180.9
1.26	2.18	99.9	165.8
1.34	2.39	116.8	152.6
1.39	2.59	131.7	150.0
1.44	2.80	145.1	130.5

https://doi.org/10.52202/077185-0031

3.2 Results related to the optimised compressor design

Figure 5 reports the results of the five configurations used for the compressor designs in Table 1. On the upper part of the graph, the radial and axial dimensions of the machine are reported to show a 2D representation of the geometry resulting from the design optimisation procedure. On the lower part, the target and actual values of PR_{ts} and $\eta_{is,ts}$ are reported to show if the required design specifications in terms of the machine's overall performance can be met. As for the compressor design targets, the PR values in Table 1 and $\eta_{is}^{c} = 0.8$ are used (to check if the cycle analysis hypotheses are valid, conservative or not achievable), interpreted as total-to-static values.

As a result, the targets specified for Configurations 1 and 2 are pessimistic because the optimised compressors can achieve better performance than those specified (and expected). For this reason, it is reasonable to assume higher COPs than that reported in Table 1 for configurations 1 and 2.

In Figure 5, Configuration 3 represents the intermediate point between the practically feasible and unfeasible configurations. In this case, according to the compressor model alone, the required performance would be close to what the single-stage compressor might achieve but still slightly unfeasible; however, also considering the uncertainty associated with the compressor model errors, it is probable that the required performance might be achieved in reality (PR_{ts} and $\eta_{is,ts}$ fall well within the model error bars). Therefore, the COP reported in Table 1 for Configuration 3 will likely be achieved and representative of what the HTHP may achieve by operating in the prescribed conditions.

Finally, the performance required to realise Configurations 4 and 5 is well beyond what the single-stage compressor can achieve, even considering the maximum extent of statistically significant model errors. In this case, the COP listed in Table 1 for Configurations 4 and 5 is not realistic and should be revised downward, given the achieved compressor efficiency.

The compressor geometric specifications resulting from the configurations in Table 1 have been listed in Table 2, together with some non-dimensional performance parameters functional to compare the found solutions with existing machines. In particular, the values of flow coefficients and Mach numbers (ϕ and Ma) align with those prescribed by (Casey and Robinson, 2021). As for work coefficient ψ, the resulting values exceeds the normal range of 0.55 – 0.8 for all the considered configurations except the first (even though the second can still be acceptable). Besides the fact that Configurations 3 to 5 could not achieve the desired PR and are characterized by low isentropic efficiencies, too-high ψ values confirm that these designs could be critical and that different specifications and/or multi-staged compressors should be used in these cases.

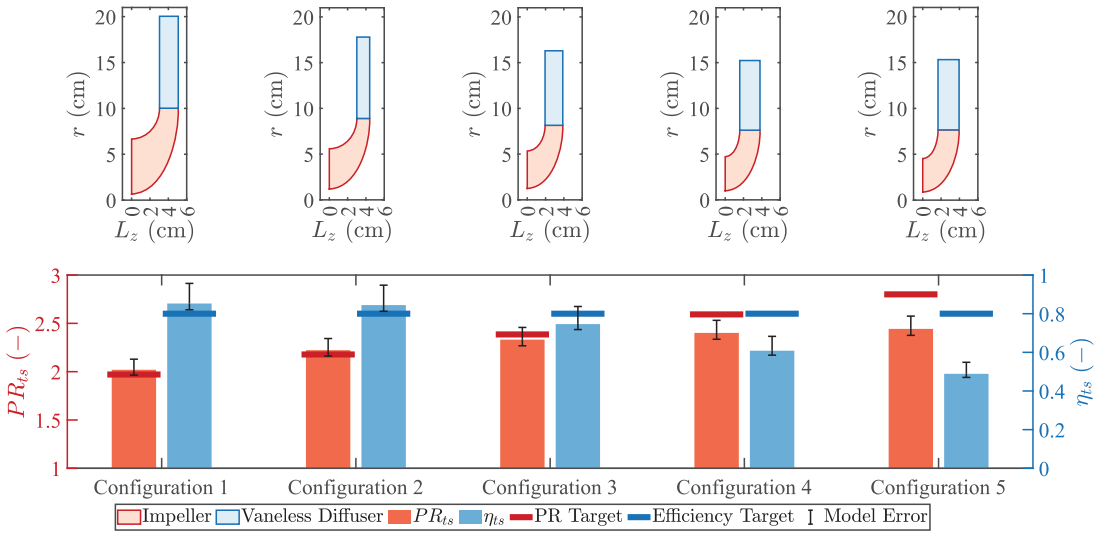

Figure 5: Compressor performance in five specific configurations. Results for T_{max} = 300 °C. On top: the compressor optimised geometry. On the bottom: Comparison between the performance achieved by the compressor design and the target performance in terms of PR_{ts} and η_{ts}.

https://doi.org/10.52202/077185-0031

Table 2: Performance and geometric specifications for the five compressor designs in Figure 5. All the compressors have p_0 = 1 bar, T_{out} = 300 °C and the inlet temperatures in Table 1.

Quantity	Config. 1	Config. 2	Config. 3	Config. 4	Config. 5
PR_{ts} (-)	2.02	2.22	2.33	2.40	2.44
PR_{tt} (-)	2.03	2.23	2.34	2.41	2.45
η_{ts} (-)	0.85	0.84	0.75	0.61	0.49
η_{tt} (-)	0.86	0.85	0.75	0.61	0.49
kRPM (-)	38.13	42.93	46.88	50.16	49.89
$\psi_{is} = (\Delta h_0)_{is}/u_2^2$ (-)	0.65	0.73	0.75	0.76	0.76
$\psi = \Delta h_0/u_2^2$ (-)	0.76	0.86	1.01	1.25	1.55
$\phi = \dot{m}/\rho_{01}D_2^2u_2$ (-)	0.099	0.098	0.097	0.096	0.084
Ma_1 (-)	0.28	0.34	0.31	0.35	0.34
Ma_2 (-)	0.67	0.78	0.78	0.79	0.79
$Ma_{1s,rel} = w_{1s}/\sqrt{kRT_1}$ (-)	0.69	0.69	0.71	0.71	0.68
$Ma_{u2} = u_2/\sqrt{kRT_{01}}$ (-)	0.94	0.95	0.97	0.98	0.99
u_2 (m/s)	400	400	400	400	400
$\beta_{1b,rms}$ (°)	-48.0	-41.3	-45.8	-41.8	-41.8
β_{2b} (°)	-32.8	-7.8	-5.0	-5.0	-5.0
r_{1s} (m)	0.067	0.056	0.053	0.047	0.045
r_{1h} (m)	0.007	0.012	0.012	0.010	0.009
r_2 (m)	0.100	0.089	0.081	0.076	0.077
r_3 (m)	0.200	0.178	0.163	0.152	0.153
$b_2 = b_3$ (m)	0.020	0.014	0.019	0.022	0.023
N_b (-)	17	18	18	19	19

4 CONCLUSIONS

This study explores a Brayton HTHP system operating with air and with a thermal capacity of 100 kWth to determine its COP under the constraints of feasible heat exchanger sizes and basic (single-stage) compressor designs. A theoretical model of the HTHP cycle was created to specify the compressor's requirements, including inlet conditions, flow rate, and pressure ratio. Several cycle configurations of practical relevance were chosen for in-depth compressor design using a validated 1-D model.

The findings offer valuable insights into the attainable performance of small-scale Brayton HTHP systems and can be summarised as follows:

- The study mapped the overall performance of Brayton HTHP, highlighting key drivers for performance regarding heat exchanger dimensions, operating temperatures and compressor performance requirements. According to the analysis, for heat production at temperatures up to 300 °C, a COP of 1.44 could be expected by operating with ε_{ihx} = 0.8, PR = 2.8 and a minimum cycle temperature of around -27 °C.
- Optimised compressor designs met targeted performance specifications in some configurations, providing insights into the realistic capabilities of small-scale Brayton HTHPs and paving the way for future advancements in HTHP cycle design and analysis. In particular, the results suggest that COP not higher than 1.34 can realistically be achieved for heat production at temperatures up to 300 °C with a single-stage centrifugal compressor and ε_{ihx} = 0.8.
- Some compressor designs resulting from the optimisation are characterised by non-dimensional performance parameters in line with the scientific literature, suggesting the practical realisability of those solutions.

https://doi.org/10.52202/077185-0031

NOMENCLATURE

Acronyms

HTHP	High-Temperature Heat Pump
COP	Coefficient of Performance
PR	Pressure Ratio

Symbols

b	Blade height	(m)
c	Absolute velocity	(m/s)
h	Ethalpy	(J/kg/K)
k	isentropic exponent	(-)
$\dot{m}$	mass flow rate	(kg/s)
p	Pressure	(Pa)
$\dot{Q}$	Heat Flow Rate	(kW)
r	Radius	(m)
T	Temperature	(K)
u	Tangential Velocity	(m/s)
w	Relative velocity	(m/s)

Greek Symbols

α	Absolute velocity flow angle	(rad)
β	Relative velocity flow angle	(rad)
ϕ	Flow coefficient	(-)
ψ	Work coefficient	(-)
ρ	Density	(kg/m^3)
σ	Slip Factor	(-)
ε	Heat exchanger effectiveness	(-)

Subscript and Superscript

0(·)	Total quantity
1,1*,…5	Compressor sections 1…5
b	Compressor Blade
ihx	Internal heat exchanger
is	Isentropic
m	Meridional
t	turbine
c	compressor
ts	Total-to-static
tt	Total-to-total
u	Tangential

REFERENCES

Arpagaus, C., Bless, F., Uhlmann, M., Schiffmann, J., and Bertsch, S. S. (2018). High temperature heat pumps: Market overview, state of the art, research status, refrigerants, and application potentials. *Energy* 152, 985–1010. doi:10.1016/j.energy.2018.03.166.

Aungier, R. H. (2000). *Centrifugal Compressors: A Strategy for Aerodynamic Design and Analysis*. ASME Press doi:10.1115/1.800938.

Bell, I. H., Wronski, J., Quoilin, S., and Lemort, V. (2014). Pure and Pseudo-pure Fluid Thermophysical Property Evaluation and the Open-Source Thermophysical Property Library CoolProp. *Ind. Eng. Chem. Res.* 53, 2498–2508. doi:10.1021/ie4033999.

Bergamini, R., Jensen, J. K., and Elmegaard, B. (2019). Thermodynamic competitiveness of high temperature vapor compression heat pumps for boiler substitution. *Energy* 182, 110–121. doi:10.1016/j.energy.2019.05.187.

Bless, F., Arpagaus, C., Bertsch, S. S., and Schiffmann, J. (2017). Theoretical analysis of steam generation methods - Energy, CO 2 emission, and cost analysis. *Energy* 129, 114–121. doi:10.1016/j.energy.2017.04.088.

Casey, M., and Robinson, C. (2021). *Radial Flow Turbocompressors Design, Analysis and Applications*. , ed. Cambridge University Press Cambridge Available at: https://lccn.loc.gov/2020046835.

Gai, L., Varbanov, P. S., Walmsley, T. G., and Klemeš, J. J. (2020). Critical Analysis of Process Integration Options for Joule-Cycle and Conventional Heat Pumps. *Energies* 13, 635. doi:10.3390/en13030635.

Gollasch, J., Lockan, M., Stathopoulos, P., and Nicke, E. (2024). Multidisciplinary Optimization of Thermodynamic Cycles for Large-Scale Heat Pumps With Simultaneous Component Design. *J. Eng. Gas Turbines Power* 146, 1–35. doi:10.1115/1.4063637.

Khoshkalam, N., Mojaddam, M., and Pullen, K. R. (2019). Characterization of the Performance of a Turbocharger Centrifugal Compressor by Component Loss Contributions. *Energies* 12, 2711. doi:10.3390/en12142711.

Manuel, S. D., Floris, T., Kira, W., Jos, S., and André, F. (2022). High technical and temporal resolution integrated energy system modelling of industrial decarbonisation. *Adv. Appl. Energy* 7, 100105. doi:10.1016/j.adapen.2022.100105.

https://doi.org/10.52202/077185-0031

Marina, A., Spoelstra, S., Zondag, H. A., and Wemmers, A. K. (2021). An estimation of the European industrial heat pump market potential. *Renew. Sustain. Energy Rev.* 139, 110545. doi:10.1016/j.rser.2020.110545.

Meroni, A., Zühlsdorf, B., Elmegaard, B., and Haglind, F. (2018). Design of centrifugal compressors for heat pump systems. *Appl. Energy* 232, 139–156. doi:10.1016/j.apenergy.2018.09.210.

Oh, H. W., Yoon, E. S., and Chung, M. K. (1997). An optimum set of loss models for performance prediction of centrifugal compressors. *Proc. Inst. Mech. Eng. Part A J. Power Energy* 211, 331–338. doi:10.1243/0957650971537231.

Schlosser, F., Jesper, M., Vogelsang, J., Walmsley, T. G., Arpagaus, C., and Hesselbach, J. (2020). Large-scale heat pumps: Applications, performance, economic feasibility and industrial integration. *Renew. Sustain. Energy Rev.* 133, 110219. doi:10.1016/j.rser.2020.110219.

Unterluggauer, J., Sulzgruber, V., Kroiss, C., Riedl, J., Jentsch, R., and Willinger, R. (2023). Design for a Heat Pump with Sink Temperatures of 200 °C Using a Radial Compressor. *Energies* 16, 4916. doi:10.3390/en16134916.

Walden, J. V. M., Bähr, M., Glade, A., Gollasch, J., Tran, A. P., and Lorenz, T. (2023). Nonlinear operational optimization of an industrial power-to-heat system with a high temperature heat pump, a thermal energy storage and wind energy. *Appl. Energy* 344, 121247. doi:10.1016/j.apenergy.2023.121247.

White, A. J. (2009). Thermodynamic analysis of the reverse Joule–Brayton cycle heat pump for domestic heating. *Appl. Energy* 86, 2443–2450. doi:10.1016/j.apenergy.2009.02.012.

Wierzbicki, A. P. (1980). "The Use of Reference Objectives in Multiobjective Optimization," in, 468–486. doi:10.1007/978-3-642-48782-8_32.

Wiesner, F. J. (1967). A Review of Slip Factors for Centrifugal Impellers. *J. Eng. Power* 89, 558–566. doi:10.1115/1.3616734.

Xu, C., and Amano, R. S. (2012). Empirical Design Considerations for Industrial Centrifugal Compressors. *Int. J. Rotating Mach.* 2012, 1–15. doi:10.1155/2012/184061.

Zhang, C., Dong, X., Liu, X., Sun, Z., Wu, S., Gao, Q., et al. (2019). A method to select loss correlations for centrifugal compressor performance prediction. *Aerosp. Sci. Technol.* 93, 105335. doi:10.1016/j.ast.2019.105335.

Zühlsdorf, B., Bühler, F., Bantle, M., and Elmegaard, B. (2019). Analysis of technologies and potentials for heat pump-based process heat supply above 150 °C. *Energy Convers. Manag. X* 2, 100011. doi:10.1016/j.ecmx.2019.100011.

ACKNOWLEDGEMENT

This research has received a financial contribution from the National Recovery and Resilience Plan (PNRR), Mission 4 Component 2 Investment 1.3 - Call for tender No. 1561 of 11.10.2022 of Ministero dell'Università e della Ricerca (MUR); funded by the European Union – NextGenerationEU.

Dr. Guido Francesco Frate acknowledges the financial contribution received by the Ministry of University and Research (MUR) as part of the FSE REACT-EU - PON 2014-2020 "Research and Innovation" resources – Green/Innovation Action - DM MUR 1062/2021 - Title of the Research: *Soluzione e tecnologie innovative per la generazione di potenza e le macchine a fluido nella transizione verde*.

SUPPLEMENTARY MATERIALS

The compressor model described in the paper can be downloaded at the following link:

https://github.com/guidoffrate/Centrifugal-compressor-model

https://doi.org/10.52202/077185-0031